Journal of Statistical Physics, Vol. 81, Nos. 1/2, 1995

Direct Assessment of Lattice Boltzmann Hydrodynamics and Boundary Conditions for Recirculating Flows

David R. Noble,[1] John G. Georgiadis,[1] and Richard O. Buckius[1]

Received November 2, 1994; final February 23, 1995

A hydrodynamic boundary condition is developed for lattice Boltzmann hydrodynamics using a square, orthogonal grid. A constraint based on energy considerations is developed to provide closure for the equations which govern the particle distribution at the boundaries. This boundary condition is applied to the two-dimensional, steady flow of an incompressible fluid behind a grid, known as Kovasznay flow. The results are compared to those using alternate boundary conditions using the known exact solution. The hydrodynamic boundary condition produces quadratic spatial convergence, while alternate techniques fail to maintain this second-order accuracy.

KEY WORDS: Lattice Boltzmann; boundary condition.

1. INTRODUCTION

Like its predecessor, lattice gas automata,[1] the lattice Boltzmann method (LBM)[2-6] is a relatively new technique for studying fluid mechanics using parallel computers. Schemes based on the LBM have two distinct advantages over conventional numerical methods: (1) they do not require the generation of cumbersome boundary-conforming numerical grids, and (2) they are naturally parallelizable and easily executed using massively parallel computers. The LBM deserves careful evaluation in view of the demonstrated inefficiency of conventional computational schemes, and also for its potential in probing novel physical phenomena governed by the discrete Boltzmann equation.

Enthusiasm for the LBM is mitigated, however, by boundary condition implementation difficulties. Formally, the accuracy of a given numerical

[1] Department of Mechanical and Industrial Engineering, University of Illinois, Urbana, Illinois 61801.

0022-4715/95/1000-0017$07.50/0

implementation of boundary conditions can be quantified by the slope of asymptotic error decay as the numerical grid is refined. The simple "bounce-back" boundary condition gives generally first-order accuracy.[7–10] Shordos[11] suggested a finite-difference scheme to impose boundary and initial conditions which are formally second-order accurate in space and time. Noble *et al.*[12] recently proposed a rigorous hydrodynamic boundary condition which extends the second-order spatial accuracy of the LBM from the bulk region to the boundary nodes.

In Noble *et al.*[12] the proposed boundary condition was implemented successfully for flows involving velocity gradients in a single direction. The objective of this work is to develop an additional constraint based on energy considerations, and to put this implementation to a severe test by focusing on a more complex flow field. The accuracy of the scheme is assessed here in two ways: (1) *a priori*, by building a theoretical foundation for the proposed boundary condition closure scheme, and (2) *a posteriori*, by direct comparison of the LBM numerical solution with an exact solution of the two-dimensional Navier–Stokes equations for a recirculating flow, known as Kovasznay flow.

2. THEORY

2.1. Lattice Boltzmann Hydrodynamics

The lattice Boltzmann method employed in this study uses an othogonal, square lattice in which each node has eight nearest neighbors. The lattice incorporates horizontal and vertical links of unit length and diagonal links of length $\sqrt{2}$. A vector is assigned for each direction,

$$\mathbf{e}_i = |\mathbf{e}_i| \left(\cos \frac{2\pi(i-1)}{8}, \sin \frac{2\pi(i-1)}{8} \right), \qquad i = 1, 2, \ldots, 8 \tag{1}$$

where $|\mathbf{e}_i| = 1$ for the horizontal and vertical directions ($i = 1, 3, 5, 7$) and $|\mathbf{e}_i| = \sqrt{2}$ for the diagonal directions ($i = 2, 4, 6, 8$). The particle distribution $f_i(\mathbf{x}, t)$ is the probability of finding a particle at location $\mathbf{x}$ and time t that is moving in direction $\mathbf{e}_i$. Also included in the distribution is a rest particle contribution $f_0(\mathbf{x}, t)$. The primary variables, density and velocity, are found from this particle distribution according to the relations

$$\sum_i f_i = \rho \tag{2}$$

$$\sum_i f_i \mathbf{e}_i = \rho \mathbf{u} \tag{3}$$

A measure of the kinetic energy κ is also found according to

$$\tfrac{1}{2}\sum_i (\mathbf{e}_i \cdot \mathbf{e}_i) f_i = \rho\kappa \tag{4}$$

The difference between this microscopic kinetic energy and the energy of the macroscopic velocity field is the internal energy ε:

$$\rho\varepsilon = \tfrac{1}{2}\sum_i (\mathbf{e}_i - \mathbf{u})^2 f_i = \rho\kappa - \tfrac{1}{2}\rho(u^2 + v^2) \tag{5}$$

where u, v are the Cartesian components of the two-dimensional velocity field. The present LBM, like lattice gas models, corresponds to a probabilistic description of the fluid particle microhydrodynamics, based on kinetic theory. Equations (2)–(4) represent the first three moments of f which follow from the discrete probabilistic formalism associated with a discrete lattice, such as that defined in Eq. (1).

The Boltzmann equation is integrated in the form

$$f_i(\mathbf{x} + \mathbf{e}_i, t+1) = f_i(\mathbf{x}, t) + \Omega_i(f(\mathbf{x}, t)) \tag{6}$$

The above equation describes the evolution of the particle distribution function from two contributions, a collision term and a streaming term. The streaming term models the advection of the particle distribution from a reference node to its nearest neighbor in the direction of its velocity $\mathbf{e}_i$. The second term Ω_i represents the local change in the particle distribution owing to particle collision. Utilizing the linearized, single-time relaxation model of Bhatnagar *et al.*[13] applied to the lattice Boltzmann,[5] we can write the collision operator as

$$\Omega_i(f) = -\frac{1}{\tau}(f_i - f_i^{\mathrm{eq}}) \tag{7}$$

Using this simplification, we can write the lattice Boltzmann evoluation equation as

$$f_i(\mathbf{x} + \mathbf{e}_i, t+1) = f_i(\mathbf{x}, t) + \frac{1}{\tau}(f_i^{\mathrm{eq}}(\mathbf{x}, t) - f_i(\mathbf{x}, t)) \tag{8}$$

Using this technique, we reduce the solution of the fluid equations to two major steps. First, in a collision step the distributions undergo relaxation toward equilibrium according to the right-hand side of Eq. (7). Second, the particle distributions stream to their nearest neighbors.

The equilibrium particle distribution is selected so that the continuum fluid equations (conservation of mass and momentum) are recovered when the Boltzmann transport equation is truncated to its long-wavelength and low-frequency limit. The equilibrium distribution used in this work is

$$f_0^{eq} = \rho[\tfrac{2}{7} - \tfrac{2}{3}(\mathbf{u}\cdot\mathbf{u})] \tag{9}$$

$$f_i^{eq} = \rho[\tfrac{1}{7} + \tfrac{1}{3}(\mathbf{e}_i\cdot\mathbf{u}) + \tfrac{1}{2}(\mathbf{e}_i\cdot\mathbf{u})^2 - \tfrac{1}{6}(\mathbf{u}\cdot\mathbf{u})], \qquad i = 1, 3, 5, 7 \tag{10}$$

$$f_i^{eq} = \rho[\tfrac{1}{28} + \tfrac{1}{12}(\mathbf{e}_i\cdot\mathbf{u}) + \tfrac{1}{8}(\mathbf{e}_i\cdot\mathbf{u})^2 - \tfrac{1}{24}(\mathbf{u}\cdot\mathbf{u})], \qquad i = 2, 4, 6, 8 \tag{11}$$

where f_i^{eq} is the equilibrium distribution of particles moving in direction i and f_0^{eq} is the equilibrium distribution of rest particles. A recapitulation of the theoretical steps involved in the derivation of the LBM is given in the following section.

2.2. Recovery of the Macroscopic Equations by the Chapman–Enskog Expansion

The basic procedure linking the discrete kinetic equation, Eq. (6), to the macroscopic equations, following the methodology and terminology of Alexander *et al.*[14] produces an explicit form for the fluid thermophysical parameters, such as the viscosity and the speed of sound. A power series expansion of the local equilibrium distribution f^{eq} in terms of the macroscopic local velocity $\mathbf{u}$, followed by a Taylor series expansion of Eq. (6) to second order in space and time, is supplemented by an expansion of the particle distribution function around its equilibrium value. This version of the Chapman–Enskog expansion generates a hierarchy of kinetic equations for the particle distribution function. Forming the first and second moments of the first- and second-order kinetic equations and neglecting terms $O(|\mathbf{u}|^3)$ produces the mass and momentum (Navier–Stokes) equations if the coefficients of the equilibrium distribution are appropriately constrained. For the square lattice used here [Eq. (1)], the solution expressed in Eqs. (9)–(11) satisfies all the constraints. This distribution is identical with that used by Skordos.[11] The kinematic viscosity of the fluid ν and speed of sound c_s are given respectively by

$$\nu = \frac{2\tau - 1}{6} \tag{12}$$

and

$$c_s = \sqrt{3/7} \tag{13}$$

Unlike the case of the hexagonal grid used by Noble *et al.*,[12] there is an independent macroscopic energy equation for the square grid employed here. However, owing to the lack of extra degrees of freedom [constrained by the truncation level in Eqs. (9)–(11)], the energy conservation equation, complete with Fourier conduction as in Alexander *et al.*,[14] cannot be completely recovered. Nevertheless, it is useful, as shown in the following section, to examine the energy conservation law implied by our implementation of LBM. Forming the third moment of the first- and second-order kinetic equations and neglecting terms $O(|\mathbf{u}|^3)$ results in

$$\varepsilon = c_S^2 - \tau c_S^2(\nabla \cdot \mathbf{u})\delta + O(\delta^2) \tag{14}$$

for the steady-state hydrodynamic field, where δ is a small quantity which is proportional to the Knudsen number. This states that for a low Mach number and a low Knudsen number, the internal energy is equal to the square of the sound speed. This property is exploited to provide closure to the problem of defining consistent boundary conditions, as shown in the following section.

2.3. Hydrodynamic Boundary Conditions

In order to simulate boundary value problems using the lattice Boltzmann method, boundary conditions for the particle distribution must be developed. The consistent hydrodynamic approach, first proposed by Noble *et al.*,[12] seeks to develop a complete set of constraints for the particle distribution such that a specified velocity profile is maintained on the boundaries. During each time step in the LBM procedure, the collision and streaming processes modify the particle distribution at each node. The goal of the hydrodynamic approach is to prescribe this process in such a fashion that the desired velocity conditions are satisfied at the end of the time step.

The general theory for hydrodynamic boundary conditions for a hexagonal lattice has been developed.[12] In this work, a constraint based on internal energy is developed in order to prescribe the unknown components of the square-lattice particle distribution function. In developing the hydrodynamic boundary condition it is helpful to distinguish between the three types of lattice nodes involved in a lattice Boltzmann simulation. First, nodes which lie wholly within the fluid are termed interior, or fluid nodes (denoted by subscript f). Second, nodes which lie just outside of the boundary of the fluid domain are termed wall nodes (denoted by subscript w). Last, nodes on the boundary between the fluid mass and the wall mass are the boundary nodes (denoted by subscript b). Thus, the neighbors of a boundary node are classified in three groups:

$\mathbf{x}_b - \mathbf{e}_{f\to b}$ Neighbors of the boundary node which lie within the fluid

$\mathbf{x}_b - \mathbf{e}_{b\to b}$ Neighbors of the boundary node which lie on the boundary

$\mathbf{x}_b - \mathbf{e}_{w\to b}$ Neighbors of the boundary node which lie within the wall

where the difference notation represents direction and the eight lattice directions are classified in three groups. The notation $f\to b$ is used to denote directions from neighboring fluid nodes to the boundary node of interest. Likewise, $b\to b$ denotes directions from neighboring boundary nodes to the boundary node of interest and $w\to b$ denotes directions from neighboring wall nodes to the boundary node of interest.

Constraints for the particle distribution on the boundary are derived by examining the dependence of the macroscopic quantities at a boundary node on the particle distribution. The velocity and density at a boundary at the end of a time step are found from the particle distribution at the boundary according to the expressions

$$\rho(\mathbf{x}_b, t+1) = \sum_i f_i(\mathbf{x}_b, t+1) \tag{15}$$

$$\rho(\mathbf{x}_b, t+1)\,\mathbf{u}(\mathbf{x}_b, t+1) = \sum_i f_i(\mathbf{x}_b, t+1)\cdot \mathbf{e}_i \tag{16}$$

This is written as

$$\rho(\mathbf{x}_b, t+1) = \sum_{i=w\to b} f_i(\mathbf{x}_b, t+1) + \sum_{i=f,\,b\to b} f_i(\mathbf{x}_b, t+1) \tag{17}$$

$$\rho(\mathbf{x}_b, t+1)\,\mathbf{u}(\mathbf{x}_b, t+1) = \sum_{i=w\to b} f_i(\mathbf{x}_b, t+1)\cdot \mathbf{e}_i + \sum_{i=f,\,b\to b} f_i(\mathbf{x}_b, t+1)\cdot \mathbf{e}_i \tag{18}$$

where the particle distribution has been separated into two types of contributions: components which come from wall nodes and components which come from fluid or boundary nodes. Solving for the contributions from the wall nodes produces

$$\sum_{i=w\to b} f_i(\mathbf{x}_b, t+1) = \rho(\mathbf{x}_b, t+1) - \sum_{i=f,\,b\to b} f_i(\mathbf{x}_b, t+1) \tag{19}$$

$$\sum_{i=w\to b} f_i(\mathbf{x}_b, t+1)\cdot \mathbf{e}_i = \rho(\mathbf{x}_b, t+1) - \sum_{i=f,\,b\to b} f_i(\mathbf{x}, t+1)\cdot \mathbf{e}_i \tag{20}$$

This form of the boundary condition gives the constraints on the unknown components of the particle distribution which are produced by the macroscopic velocity and density boundary conditions. Determining the individual unknown components of the distribution requires the application of these constraints for a specific lattice and boundary geometry.

The nature of the resulting constraint equations is demonstrated for a boundary node lying on a vertical boundary for which $\mathbf{e}_1$ is a unit normal to the boundary oriented into the fluid. Equations (19)–(20) yield for the new time $t+1$

$$f_1+f_2+f_8=\rho-[f_0+f_3+f_4+f_5+f_6+f_7] \tag{21}$$

$$f_1+f_2+f_8=\rho u-[-f_4-f_5-f_6] \tag{22}$$

$$f_2-f_8=\rho v-[f_3+f_4-f_6-f_7] \tag{23}$$

where u, v are the Cartesian components of the two-dimensional velocity field. As previously developed for a hexagonal grid,[12] this results in two equations, Eqs. (21) and (22), which both constrain the sum of the unknown components of the particle distribution, $f_1+f_2+f_8$. Thus, if these two equations are to be consistent, the density must considered to be an unknown quantity. This simply means that stating a specific velocity profile along a boundary fixes the density and therefore the pressure along the boundary. This is a fortuitous but beneficial result since the density is often unknown at the boundary. With the density being a calculated quantity, however, the system is underconstrained. Equations (21)–(23) represent only three equations constraining the four quantities f_1, f_2, f_8 and ρ. A fourth constraint is needed to provide closure to this problem.

Motivated by Eq. (14), closure is provided by maintaining a fixed internal energy at the boundary. The internal energy at a boundary at the end of a time step is found from

$$\begin{aligned}&\rho(\mathbf{x}_b, t+1)\,\varepsilon(\mathbf{x}_b, t+1)\\&\quad=\rho(\mathbf{x}_b, t+1)\,\kappa(\mathbf{x}_b, t+1)+\tfrac{1}{2}\rho[u^2(\mathbf{x}_b, t+1)+v^2(\mathbf{x}_b, t+1)]\end{aligned} \tag{24}$$

where κ is the kinetic energy,

$$\rho(\mathbf{x}_b, t+1)\,\kappa(\mathbf{x}_b, t+1)=\tfrac{1}{2}\sum_i(\mathbf{e}_i\cdot\mathbf{e}_i)\,f_i(\mathbf{x}_b, t+1) \tag{25}$$

This is written as

$$\begin{aligned}&\rho(\mathbf{x}_b, t+1)\,\varepsilon(\mathbf{x}_b, t+1)+\tfrac{1}{2}\rho[u^2(\mathbf{x}_b, t+1)+v^2(\mathbf{x}_b, t+1)]\\&\quad=\tfrac{1}{2}\sum_{i=w\to b}(\mathbf{e}_i\cdot\mathbf{e}_i)\,f_i(\mathbf{x}_b, t+1)+\tfrac{1}{2}\sum_{i=f,\,b\to b}(\mathbf{e}_i\cdot\mathbf{e}_i)\,f_i(\mathbf{x}_b, t+1)\end{aligned} \tag{26}$$

where the particle distribution is again separated into types of contributions: components which come from wall nodes and components which

come from fluid or boundary nodes. Solving for the contributions from the wall nodes produces

$$\sum_{i=\mathrm{w}\to\mathrm{b}} (\mathbf{e}_i\cdot\mathbf{e}_i)\, f_i(\mathbf{x}_\mathrm{b}, t+1)$$
$$= 2\rho(\mathbf{x}_\mathrm{b}, t+1)\,\varepsilon(\mathbf{x}_\mathrm{b}, t+1) + \rho[u^2(\mathbf{x}_\mathrm{b}, t+1) + v^2(\mathbf{x}_\mathrm{b}, t+1)]$$
$$- \sum_{i=\mathrm{f},\,\mathrm{b}\to\mathrm{b}} (\mathbf{e}_i\cdot\mathbf{e}_i)\, f_i(\mathbf{x}_\mathrm{b}, t+1) \tag{27}$$

When applied to the boundary node on a vertical boundary, this constraint yields

$$f_1 + 2f_2 + 2f_8 = 2\rho\varepsilon + \rho(u^2+v^2) - [f_3 + 2f_4 + f_5 + 2f_6 + f_7] \tag{28}$$

The system is now fully constrained through Eqs. (21)–(23) and (28). The density and unknown components of the particle distribution are found using these constraints, which have been developed on the basis of the velocity boundary conditions and fixed internal energy.

2.4. Alternate Boundary Conditions

Finite-difference-based boundary conditions developed by Skordos[11] provide an alternate technique for imposing boundary conditions for lattice Boltzmann simulations. The finite-difference-based boundary condition includes additional terms in the equilibrium distribution so that the fluid viscosity can be modified independently of the relaxation parameter. This allows the relaxation parameter to be set to unity, and thus the particle distribution is replaced by the modified equilibrium distribution during the collision step. In this scheme[11] the normal collision process is used for all internal nodes and the modified collision operator is used at the boundaries. The net result is that the particle distribution at the boundaries is replaced during the collision step by a modified equilibrium distribution of the form

$$f_0^{*\mathrm{eq}} = f_0^{\mathrm{eq}} - \frac{2(1-\tau)}{7}(\nabla\cdot\rho\mathbf{v}) \tag{29}$$

$$f_i^{*\mathrm{eq}} = f_i^{\mathrm{eq}} + \frac{1-\tau}{3}[\mathbf{e}_i\cdot\nabla(\mathbf{e}_i\cdot\rho\mathbf{v})] - \frac{1-\tau}{7}(\nabla\cdot\rho\mathbf{v}), \qquad i=1,3,5,7 \tag{30}$$

$$f_i^{*\mathrm{eq}} = f_i^{\mathrm{eq}} + \frac{1-\tau}{12}[\mathbf{e}_i\cdot\nabla(\mathbf{e}_i\cdot\rho\mathbf{v})] - \frac{1-\tau}{28}(\nabla\cdot\rho\mathbf{v}), \qquad i=2,4,6,8 \tag{31}$$

This distribution has terms which involve gradients of density and velocity. For general flows where exact expressions for these gradients are unknown,

these terms must be evaluated using finite differences. In the simulations reported here, second-order accurate asymmetric differences are used at the boundaries to evaluate these terms.

Another alternate boundary condition involves imposing the unmodified equilibrium distribution at the boundaries during the collision step. The method is expected to be accurate for relaxation parameter values near unity, since the collision process simply replaces the particle distribution with the equilibrium distribution when the relaxation parameter is set to unity. There is no reason to expect, however, that this method will perform well for arbitrary values of the relaxation parameter.

3. RESULTS

Laminar flow behind a two-dimensional grid, known as Kovasznay flow,[15] is investigated. The exact solution derived by Kovasznay is written as

$$u^*(x, y) = U_0 \left[1 - e^{-\lambda x/L} \cos\left(\frac{2\pi y}{L}\right) \right] \tag{32}$$

$$v^*(x, y) = U_0 \left[\frac{\lambda}{2\pi} e^{-\lambda x/L} \sin\left(\frac{2\pi y}{L}\right) \right] \tag{33}$$

$$p^*(x, y) = \frac{1}{2}(1 - e^{-2\lambda x/L}) \tag{34}$$

where

$$\lambda = \left[\frac{Re^2}{4} + 4\pi^2 \right]^{1/2} - \frac{Re}{2} \tag{35}$$

and the Reynolds number Re is defined as

$$Re = \frac{U_0 L}{\nu} \tag{36}$$

where U_0 is the maximum fluid velocity and L is half the vertical length of the computational domain. The flow is simulated for the region $-1/2 \leqslant x/L \leqslant 2$ and $-1/2 \leqslant y/L \leqslant 3/2$.

From the exact solution it is apparent that the flow is periodic in the y direction. Taking advantage of this feature of the solution, we apply periodic boundary conditions along the horizontal boundaries of the domain. This is accomplished by allowing the particle populations that stream out of the domain through the upper or lower surface to reenter on the opposite side.

The vertical boundaries are modeled using Dirichlet boundary conditions in which the exact solution is imposed at the inlet and outlet. These Dirichlet boundary conditions are implemented using the hydrodynamic boundary condition (HBC) developed here. For comparison, the flow is also simulated using the finite-difference-based boundary condition (FDBC)[11] and the equilibrium distribution boundary condition (FEQBC) at the inlet and outlet. For all simulations presented here, the density at the boundary is calculated based on the velocity–pressure consistency relationship expressed in Eqs. (26)–(27). This allows the various methods to be compared on an equal basis. An additional consequence is that all three methods produce identical results when the relaxation parameter is set to unity.

Figure 1 shows the steady-state sreamlines for $Re = 40$ simulated with a 80×64 computational grid utilizing the hydrodynamic boundary condition presented here. Two recirculation regions are formed within the computational domain, and the flow reattaches and is nearly parallel at the exit of the domain. As the Reynolds number increases, the recirculation region extends further into the domain. It is also noteworthy that the gradients in the x direction decrease with increasing Reynolds number, while the

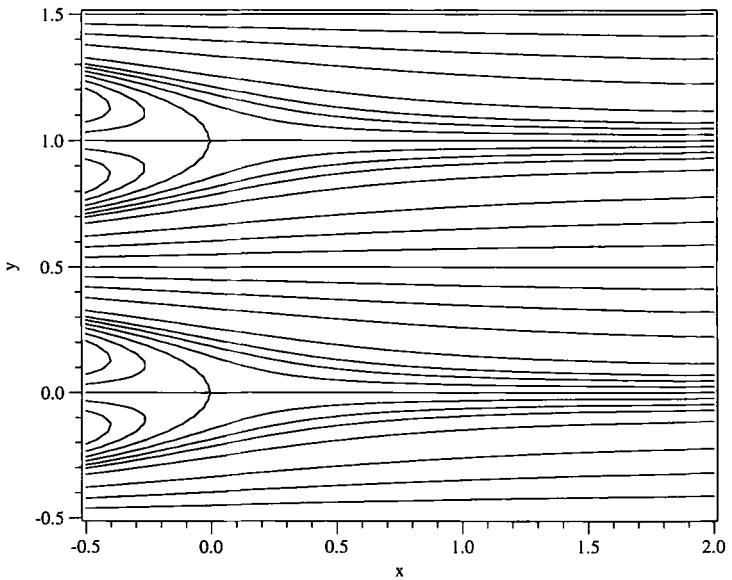

Fig. 1. Streamlines for Kovasznay flow simulation using the hydrodynamic boundary condition which maintains constant internal energy. The relaxation parameter is $\tau = 0.58$. The resulting maximum error in velocity is $E_V = 3.43 \times 10^{-3}$ with a maximum deviation in internal energy of $E_\varepsilon = 8.80 \times 10^{-6}$.

gradients in the y direction are independent of flow parameters. Thus, this flow can be more accurately simulated computationally for higher Reynolds numbers.

The hydrodynamic boundary condition, the finite-difference-based boundary condition, and the equilibrium distribution boundary condition are used to simulate Kovasznay flow at small Reynolds number ($Re = 0.1$) for 20×16, 40×32, and 80×64 computational grids. The flowfield is initialized using the equilibrium particle distribution for stationary flow. The boundary conditions are then enforced, and the solution is marched in time until steady state is achieved. These calculations are performed using the CM-5 at the National Center for Supercomputing Applications. Using a 64-node partition, an 80×64 domain is simulated for the hydrodynamic boundary condition and the equilibrium distribution boundary condition in approximately 135,000 time steps and 30 min of cpu time. The finite-difference-based boundary condition requires a similar number of time steps, but uses about 2.75 times as much time due to the cpu-intensive finite-difference operations needed to calculate the modified equilibrium distribution.

When the simulations reach steady state, the error is calculated using the exact analytical solution u^* and v^*. A pointwise relative velocity error is defined as

$$E_V = \frac{[(u-u^*)^2 + (v-v^*)^2]^{1/2}}{U_0} \tag{37}$$

The relative deviation in the internal energy is computed at each location by the formula

$$E_\varepsilon = \frac{|\varepsilon - \varepsilon_0|}{\varepsilon_0} \tag{38}$$

where

$$\varepsilon_0 = \tfrac{3}{7}$$

is the internal energy for the equilibrium distribution which is used to initialize the simulation. The Mach number is defined as the ratio of the maximum fluid velocity U_0 to the speed of sound c_s,

$$M = \frac{U_0}{c_s} = \frac{U_0}{\sqrt{3/7}} \tag{39}$$

The accuracy of the simulations, however, is a function of the computational Mach number, which is defined relative to the lattice Boltzmann

propagation speed c, which is unity in all of the simulations performed here,

$$M_c = \frac{U_0}{c} = U_0 \tag{40}$$

Figures 2–4 show the maximum relative velocity error over the entire domain as a function of the maximum fluid velocity or computational Mach number for $Re = 0.1$. Also shown in these figures is the maximum relative deviation in the internal energy as a function of the computational Mach number. For each trial, the Reynolds number is held constant by varying the fluid viscosity in proportion to the maximum fluid velocity.

These results may be used to assess the accuracy of the lattice Boltzmann method when applied to recirculating flows. The simulation accuracy is seen to be a function of the computatonal Mach number, the relaxation parameter, and the grid spacing. As previously noted,[11,16] the computational Mach number is of primary importance in lattice Boltzmann simulations. When the fluid velocity approaches the microscopic speed, the higher order terms in the Chapman–Enskog expansion become important.

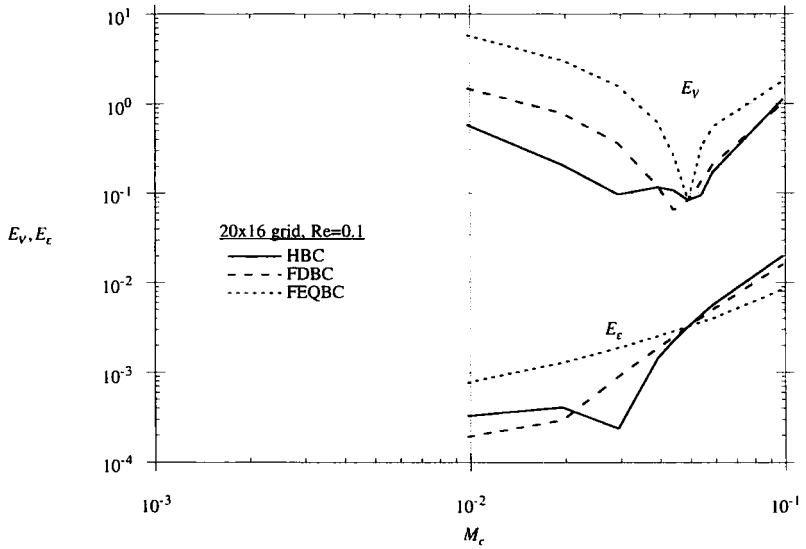

Fig. 2. Errors in velocity and deviations from constant internal energy using the hydrodynamic boundary condition (HBC), the finite-difference-based boundary condition (FDBC), and the equilibrium distribution boundary condition (FEQBC) on a 20×16 computational grid for $Re = 0.1$.

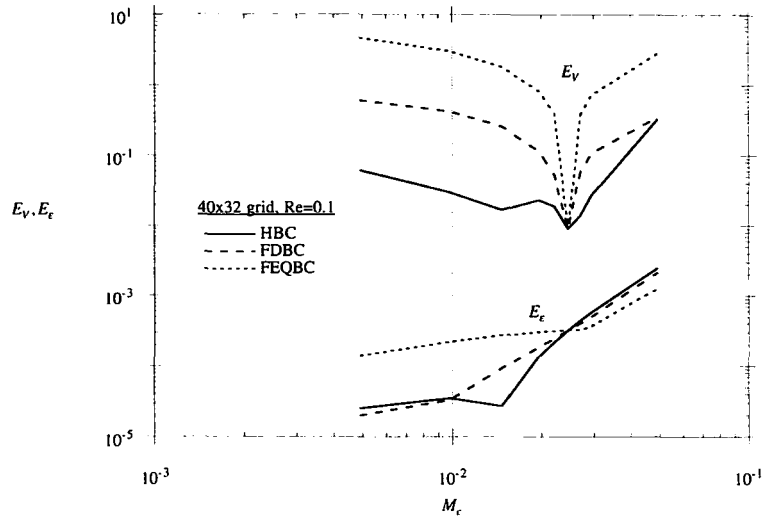

Fig. 3. Errors in velocity and deviations from constant internal energy using the hydrodynamic boundary condition (HBC), the finite-difference-based boundary condition (FDBC), and the equilibrium distribution boundary condition (FEQBC) on a 40×32 computational grid for $Re = 0.1$.

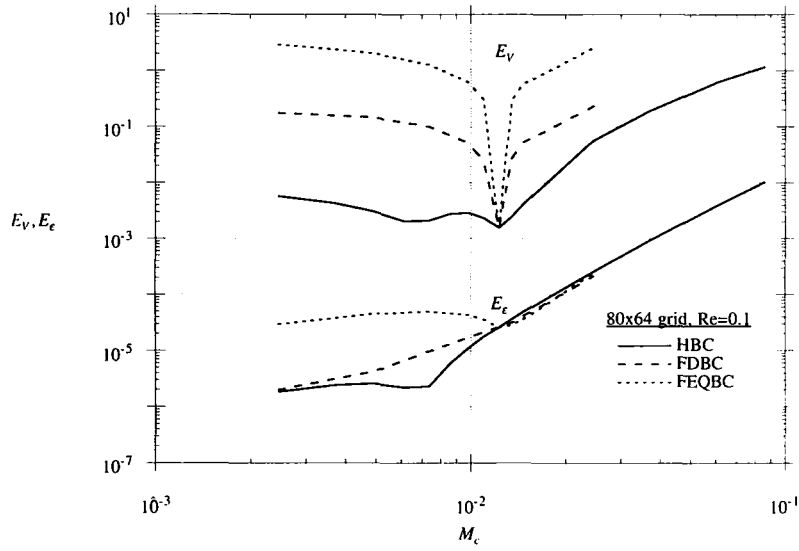

Fig. 4. Errors in velocity and deviations from constant internal energy using the hydrodynamic boundary condition (HBC), the finite-difference-based boundary condition (FDBC), and the equilibrium distribution boundary condition (FEQBC) on an 80×64 computational grid for $Re = 0.1$.

These terms can no longer be neglected, and therefore the macroscopic dynamics of the system fails to simulate the Navier–Stokes equations.

The relaxation parameter also has a large effect on the accuracy of a lattice Boltzmann simulation. When the error due to finite computational Mach number is negligible (approximately $M_c < 0.01$), the error is seen to be a strong function of the relaxation parameter with a local minimum in the error occurring for $\tau = 1.0$.

The lattice Boltzmann scheme exhibits second-order spatial accuracy when using boundary conditions which are at least second-order accurate.[12, 13] The spatial convergence for these simulations is measured by varying the grid size while maintaining a constant Reynolds number and viscosity. Figure 5 shows the reduction in error as the grid is refined for two values of the relaxation parameter, $\tau = 0.6$, 1.5, and a constant Reynolds number of 0.1 when using the hydrodynamic boundary condition, the finite-difference-based boundary condition, and the equilibrium distribution boundary condition. From the slope of these curves it is apparent that the second-order accuracy is maintained when using the hydrodynamic boundary condition, but suffers greatly when using either of

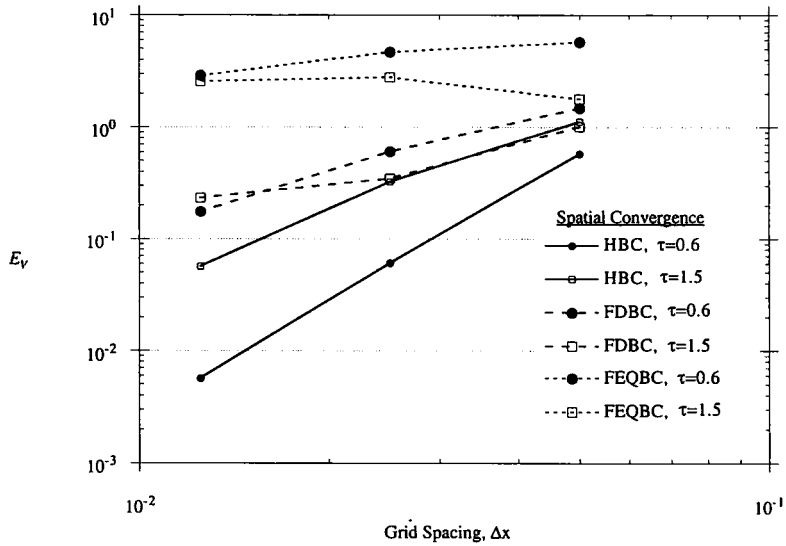

Fig. 5. Error in velocity for 20×16, 40×32, and 80×64 computational grids at $Re = 0.1$ using the hydrodynamic boundary condition (HBC), the finite-difference-based boundary condition (FDBC), and the equilibrium distribution boundary condition (FEQBC).

the alternate methods when $\tau \neq 1$. The finite-difference-based method is, however, seen to be superior to the equilibrium distribution boundary condition, which does not exhibit any convergence for $\tau > 1.1$. That is, the solution is seen to increase as the grid is refined for large values of τ when using the equilibrium distribution boundary condition.

The performances of the hydrodynamic boundary condition, the finite-difference-based boundary condition, and equilibrium distribution boundary condition are examined at moderate Reynolds number. Simulations are performed over a range of computational Mach numbers and relaxation parameters for $Re = 10$ on a 80×64 computational grid. The maximum relative velocity error is plotted as a function of computational Mach number in Fig. 6. The behavior is markedly different than that for the same grid and lower Reynolds number. In this regime, the computational Mach number is the primary source of error in the lattice Boltzmann simulation. The error is seen to decrease rapidly as the fluid velocity is decreased. Also, the effect of the relaxation parameter is no longer dominant. In fact, there is no perceptible advantage to using $\tau = 1.0$ in this moderate computational Mach number regime when using either the hydrodynamic boundary condition or the finite-difference-based boundary condition. The simulations using the hydrodynamic boundary condition are more accurate for any

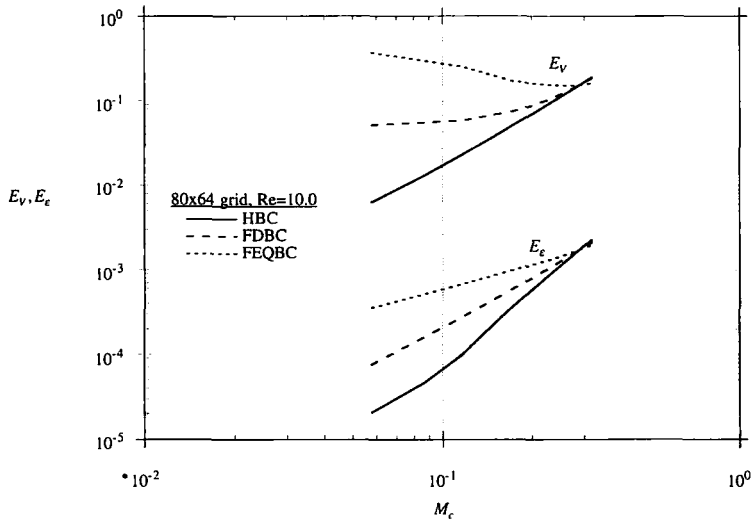

Fig. 6. Errors in velocity and deviations from constant internal energy using the hydrodynamic boundary condition (HBC), the finite-difference-based boundary condition (FDBC), and the equilibrium distribution boundary condition (FEQBC) on an 80×64 computational grid for $Re = 10$.

given value of the relaxation parameter than simulations using the alternative boundary conditions.

Assessment of the spatial dependence of the error is also possible. Although the specific distribution depends on the boundary conditions and the flow parameters, general trends pervade all runs. In all simulations and for all boundary conditions, the error in both components of velocity and the fluctuations in internal energy are, like the exact solution, periodic functions in y. The velocity error is zero on the inlet and outlet planes where the exact solution is enforced, and when using the hydrodynamic boundary condition or equilibrium distribution boundary condition, the internal energy error is also zero. The amplitude of the errors increases rapidly, however, and the maximum amplitude occurs a short distance from the inlet plane ($-0.5 < x < -0.2$). The error then decays quickly with increasing x in a manner similar to the exponential decay of the velocity gradients.

4. CONCLUSION

In this work, a hydrodynamic boundary condition for the lattice Boltzmann method applied to a square, orthogonal grid is developed. The hydrodynamic lattice Boltzmann method is shown theoretically to maintain constant internal energy under steady flow conditions. Using this constraint, in addition to those supplied by conservation of mass and momentum, we develop a complete set of simultaneous equations for prescribing the particle distribution at the boundary in terms of the velocity boundary conditions. The density (which is directly related to the pressure) is determined solely from the velocity boundary conditions; an additional explicit density boundary condition is not needed. The hydrodynamic boundary condition is applied to the recirculating Kovasznay flow for which an exact solution is available, and the results are compared with those using two alternate boundary conditions. The hydrodynamic boundary condition produces greater accuracy than the alternate methods and maintains second-order spatial convergence as the grid is refined.

ACKNOWLEDGMENTS

Discussions with Shiyi Chen are appreciated. The research was supported by a National Science Foundation Graduate Fellowship, NCSA grant CBT-930030N, NSF grant CTS-9396252, and the Richard W. Kritzer Foundation. All simulations reported here were performed at the National Center for Supercomputing Applications.

REFERENCES

1. U. Frisch, B. Hasslacher, and Y. Pomeau, Lattice-gas automata for the Navier–Stokes equation, *Phys. Rev. Lett.* **56**:2505 (1986).
2. G. McNamara and G. Zanetti, Use of the Boltzmann equation to simulate lattice-gas automata, *Phys. Rev. Lett.* **61**:2332 (1988).
3. F. Higuera and J. Jimenez, Lattice gas dynamics with enhanced collisions, *Europhys. Lett.* **9**:663 (1989).
4. H. Chen, S. Chen, and W. H. Matthaeus, Recovery of the Navier–Stokes equations using a lattice Boltzmann method, *Phys. Rev. A* **45**:R5339 (1991).
5. S. Y. Chen, H. D. Chen, D. Martinez, and W. Matthaeus, Lattice Boltzmann model for simulation of magnetohydrodynamics, *Phys. Rev. Lett.* **67**:3776 (1991).
6. Y. H. Qian, D. d'Humières, and P. Lallemand, Lattice BGK models for the Navier–Stokes equation, *Europhys. Lett.* **17**:479 (1992).
7. D. d'Humières and P. Lallemand, Numerical simulations of hydrodynamics with lattice gas automata in two dimensions, *Complex Systems* **1**:599 (1987).
8. R. Cornubert, D. d'Humières, and D. Levermore, A Knudsen layer theory for lattice gases, *Physica D* **47**:241 (1991).
9. I. Ginzbourg and P. M. Adler, Boundary flow condition analysis for the three-dimensional lattice Boltzmann model, *J. Phys. II France* **4**:191 (1994).
10. D. P. Ziegler, Boundary conditions for lattice Boltzmann simulations, *J. Stat. Phys.* **71**:1171 (1993).
11. P. A. Skordos, Initial and boundary conditions for the lattice Boltzmann method, *Phys. Rev. E* **48**:4823 (1993).
12. D. R. Noble, S. Chen, J. G. Georgiadis, and R. O. Buckius, A consistent hydrodynamic boundary condition for the lattice Boltzmann method, *Phys. Fluids* **7**:203 (1995).
13. P. Bhatnagar, E. P. Gross, and M. K. Krook, A model for collision processes in gases. I. Small amplitude processes in charged and neutral one-component systems, *Phys. Rev.* **94**:511 (1954).
14. F. J. Alexander, S. Chen, and J. D. Sterling, Lattice Boltzmann thermohydrodynamics, *Phys. Rev. E* **47**:2249 (1993).
15. L. I. G. Kovasznay, Laminar flow behind a two-dimensional grid, *Proc. Camb. Phil. Soc.* **48** (1948).
16. Y. H. Qian and S. A. Orzag, Lattice BGK model for the Navier–Stokes equation: Nonlinear deviation in compressible regimes, *Europhys. Lett.* **21**:255 (1993).